
THE DYNAMIC PROPERTIES OF THE SNAIL SOIL FROM THE LJUBLJANA MARSH

BOJAN ŽLENDER and LUDVIK TRAUNER

About the authors

Bojan Žlender
University of Maribor,
Faculty of Civil Engineering,
Smetanova 17, 2000 Maribor, Slovenia
E-mail: bojan.zlender@uni-mb.si

Ludvik Trauner
University of Maribor,
Faculty of Civil Engineering,
Smetanova 17, 2000 Maribor, Slovenia
E-mail: trauner@uni-mb.si

Abstract

A series of cyclic triaxial tests was performed on snail-soil samples with different porosities. The cyclic loading was performed with a Wykeham Farrance cyclic triaxial system. The investigation was based on a series of tests in which the following conditions were varied: the initial effective pressures (50, 100, and 150 kPa), the void ratio after consolidation (2.0–1.2) and the cyclic loading expressed by the cyclic stress ratio CSR (0.1–1.0). Measurements were made of the stress, the deformation and the pore-water pressure. The results of the tests show that interdependency exists between the geomechanical characteristics and the porosity. These relationships can be expressed as functions of the density, the porosity or the water content. It is evident from the results that the changes in the coefficient of permeability, the coefficient of consolidation, and the coefficient of volume compressibility are non-linear with respect to the changes in the porosity. However, the changes at high porosity are much greater than the changes at low porosity, and the changes of the mechanical parameters, such as the Young's modulus, Poisson's ratio, and the friction angle, are indistinct and almost linear at lower changes of porosity, and after that become non-linear. The initial void ratio e is extremely high and the snail soil is liquid after consolidation; a volume strain of $\epsilon_{vol} > 16\%$ is needed for the plastic limit state. The chemical and mineral composition, the particle size distribution and the remains of micro-organisms in the

snail soil are constants. In addition, the specific surface is independent of the porosity and the density or unit weight, the porosity and the volume strain are in the well-known correlation.

The performed cyclic triaxial tests show the dynamic characteristics of the snail soil and the influence of the porosity on the cyclic loading strength. The snail soil was recognized as a highly sensitive material. A large strain appears after the initial cycles. The pore pressure, increases already during the first cycle, to the hydrostatic part of the cyclic loading, or more (depending on CSR).

The damping ratio increases exponentially with strain, after some cycles it reach its maximum value, and after that it decreases to the asymptotic value. The reason for such behaviour is the large deformation. The maximum and asymptotic values of the damping ratio are a changed minimum with a void ratio. There is obviously no influence of the porosity on the damping ratio.

The shear modulus is described in relation to shear strain. The increasing of the pore pressure is independent of the porosity until it reaches some value of the pore-pressure ratio (>0.7). Similarly, the increasing of the shear strain becomes dependent on the void ratio until it reaches some particular value of the shear strain ($>3\%$).

The deformation and failure lines for the different porosities are determined from the relationship between the shear stress and the effective stress at some shear strain, after 10 cycles.

The relationships between the shear stress and the effective stress at some value of the pore-pressure ratio are expressed in a similar way.

Two kinds of criteria were used to determine the triggering of liquefaction during the cyclic triaxial tests: first, when the pore pressure becomes equal to the effective confining pressure, and, second, when the axial strain reaches 5% of the double amplitude.

Keywords

snail soil, cyclic triaxial test, porosity, permeability, consolidation, Young's modulus, shear modulus, damping ratio, Poisson's ratio, friction angle

1 INTRODUCTION

The Ljubljana marsh is located in the south of Ljubljana, at an elevation of 287–290 m above sea level, and covers a surface of 163 km². It is a wide tectonic sink that was formed two million years ago by a gradual depression of the area. Consequently, the local rivers deposited huge amounts of sediments there, inundating the entire marsh basin at the same time. The geological structure of the Ljubljana marsh has been studied by numerous experts. The oldest geological documents go back to the middle of the 19th century, when the first geological map of this region was drawn. Later, several other studies were performed, and today the geological structure of the marsh is well investigated. The surface layer is composed of peat with a thickness of 1–9 m. The depth of the peat is nowadays significantly smaller than in the past, due to the intensive excavations in the first half of the 20th century. Below the peat layer, there is a layer of snail soil, with a thickness of a few metres at the borders to more than 10 m in the centre of the marsh. The snail-soil layer is distinctly porous, saturated with water, and of a low bearing capacity. There are clay and sandy-gravel layers below the snail-soil layer. A layer of rocks starts at a depth of some 10 m. Ground water is located immediately below the surface.

The first detailed investigation of the rheological properties of the snail soil was performed in the Laboratory of Soil Mechanics at the Faculty of Architecture, Geodesy and Civil Engineering of the University of Ljubljana [1]. A similar investigation was later repeated in the Laboratory of Soil Mechanics (LSM), Faculty of Civil Engineering of the University of Maribor [2].

Three years ago, within a research project [3], the investigation of snail soil was repeated and upgraded. An investigation of the mineralogical and physical characteristics, as well as of the geomechanical characteristics depending on the physical characteristics was made [4]. This article briefly presents the research performed and the influence of snail-soil density on the geomechanical characteristics. The density of the snail soil was increased by draining and consolidation. It is described by the volume deformation and higher density or by its porosity and water content. A short review of the snail-soil investigation in natural and different density states was made. The basic investigation and the tests with static and cyclic loading were performed. The results of the influence of snail-soil density on its physical properties and the static and dynamic strength parameters are presented. The parameters are presented as functions of the density, the porosity, the volume deformation and the water content.

2 THE CHARACTERISTICS OF SNAIL SOIL

A set of samples was taken from the southwest region of the Ljubljana marsh. The sampling took place in a region of 3 m x 3 m at a depth of 3 m. The ground was excavated to a depth of 2.5 m and a thin-walled tube sampler was forced into the ground. Samples with a diameter of 100 mm and a height of 300 mm were immediately packed after sampling and, except for the stress level; this prevents any change in the physical properties. The ground-water level was less than 1 m under the surface in the region of the sampling.

The visual appearance of the snail-soil samples was tested with a QUANTA 200 3D environmental scanning electron microscope at the Centre for Electron Microscopy at the University of Maribor. The electron microscope is equipped with a system of double jets, i.e., electronic and ionic. Photographs were taken of the wet samples, and different blow ups were made. Some photographs of dry samples, minerals in crystallized form, and the remains of micro-organisms in the snail soil were also developed.

The specific surface of the snail soil was determined at the Chemistry Institute, Ljubljana, using the five-point BET method. The experiment involved the adsorption of liquid nitrogen with 99.9% purity and a temperature of 77K. The measurements were performed using the automatic TriStar 3000 gas-adsorption analyzer, produced by the Micromeritics Instrument Corporation, Norcross, U.S.A. The results of the test showed that the snail soil has a specific surface $A_s = 5.03 \pm 0.03 \text{ m}^2/\text{g}$.

The chemical composition of the snail soil (Fig. 1) was determined at the Centre for Electron Microscopy at the University of Maribor. Their SIRION scanning electron microscope is equipped with an Oxford INCA 350 energy-dispersive spectrometer (EDS).

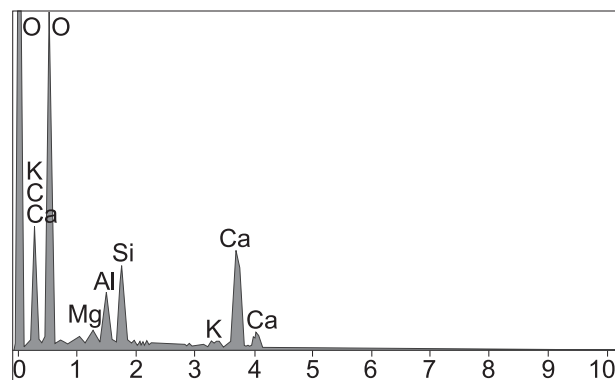


Figure 1. Chemical composition of the snail soil.

The mineral composition was determined in the Laboratory of the Geological Survey of Slovenia. The samples were scanned using the X-ray diffraction technique (XRD) with a Philips PW 3710 diffractometer, a goniometer 1820, an automatic divergence slit and a curved graphite monochromator, operating at 40 kV, 30 mA with CuK_α radiation and a Ni filter. The snail soil was composed of 87% calcite, 7% kaolinite, 4% muscovite and 3% quartz.

The physical characteristics shown in Table 1 indicate that the snail soil is saturated in nature, highly porous and almost liquid.

Table 1. The physical characteristics of snail soil.

Soil property	Symbol	Unit	Value
Plastic limit	w_p	%	37
Liquid limit	w_L	%	60
Plasticity index	I_p	%	23
Consistency index	I_c	-	-0.65
Liquidity index	I_L	-	1.65
Density of solid	ρ_s	g/cm^3	2.70
Dry unit weight	γ_d	kN/m^3	0.88
Degree of saturation	S_r	%	100

The parameters shown in Table 1 are constants. With draining and consolidation the density (unit weight), water content and void ratio are changed. The initial values (in the natural state) are shown in Table 2.

Table 2. The natural physical properties of snail soil.

Soil property	Symbol	Unit	Value
Water content	w_0	%	75
Unit weight	γ_0	kN/m^3	15.5
Void ratio	e_0	-	2.1

The grain size distribution of the snail-soil sample was determined using a Fritsch Laser Particle Sizer Analysette 22 at the Laboratory of the Geological Survey of Slovenia. The results of the grain size measurement analysis show that this snail soil falls within the range of 90% silt with respect to its granulometrical structure. The amount of clay particles is less than 10%, and there are almost no sandy particles in the snail soil.

The investigation of the compressibility was performed in the LSM. The triaxial consolidation tests were performed at different effective stresses σ_0' . The consoli-

dation parameters of the natural snail soil are given in Table 3. The values of the consolidation parameters change with a lower porosity, and the parameters can be expressed as functions of the porosity.

Table 3. Consolidation parameters of natural snail soil.

Soil property	Symbol	Unit	Value
Consolidation coefficient	c_v	m^2/year	2.8
Coefficient of volume compressibility	m_v	kPa^{-1}	$1.0-1.5 \cdot 10^{-3}$
Coefficient of soil permeability	k	m/s	$2 \cdot 10^{-9}$
Secondary compression ratio	C_α	-	0.002

The strength parameters were determined in a series of triaxial tests. The parameters of the natural snail soil are given in Table 4. The values of the parameters can also change with a lower porosity, and they can be expressed as functions of the porosity.

Table 4. The strength parameters of natural snail soil.

Soil property	Symbol	Unit	Value
Cohesion	c	kPa	0
Friction angle	φ	$^\circ$	21
Compression modulus	M_c	kPa	700-1000
Poisson's ratio	ν	-	0.4

3 EXPERIMENTATION

The following tests were performed:

- Basic investigations: visual appearance, remains of micro-organisms, specific surface, chemical and mineral composition, and physical characteristics of snail soil.
- Standard oedometer tests.
- Direct shear tests.
- Static triaxial tests: consolidated drained and undrained shear tests were performed using the Wykeham Farrance triaxial testing device.

The following strength parameters were calculated: the coefficient of permeability k , the coefficient of consolidation c_v , the coefficient of volume compressibility m_v , the compression modulus M_c , the Young's modulus E , the shear modulus G , and the Poisson's ratio ν .

The cyclic loading was performed on a Wykeham Farrance cyclic triaxial system. The basic set-up comprises:

- a load frame, capacity 100 kN;
- a triaxial pressure cell for specimens;
- a hydraulic press with electro-mechanical equipment;
- automatic hydraulic equipment and connections;
- measuring and recording equipment;
- a control and data-acquisition system;
- computer hardware and software;
- de-air watering apparatus, reservoir for de-aired water, compressor, and air-dryer.

The tests were performed under undrained conditions ($\nu = 0.5$) for a particular confining stress σ'_0 . The tested specimens were solid cylinders, 7.0 cm in diameter and 14.0 cm in height. A total of sixty-two cyclic triaxial tests were performed. The investigation was based on a series of tests in which the following conditions were varied:

- the void ratio after consolidation ... $e_c = 2.0-1.2$
- the initial effective pressures ... $\sigma'_0 = \sigma'_{3c} = 50, 100, 150$ kPa
- the cyclic loading (deviator stress) ... σ_d (t)
- the cyclic stress ratio ... $CSR = 0.1-1.0$

The following pressures were measured during the test:

- the cell pressure ... σ_{3c} (kPa)
- the back pressure ... u_b (kPa)
- the pore water pressure ... u_w (kPa)
- the axial stress in compression ... σ_z (kPa)

Measurements of the axial and volume deformations ε_z (%), ε_r (%), ε_v (%) were also taken. In the undrained tests $\varepsilon_v = 0$.

Two kinds of criteria were used to determine the liquefaction triggering during the cyclic triaxial tests: the pore pressure becoming equal to the effective confining pressure, and the axial strain reaching 5% of the double amplitude.

The following steps were observed during the testing: the preparation of the sample, the procedure for the apparatus, the performance of the test, and the interpretation of the obtained results. The investigation included drained and undrained stress-oriented three-axial tests according to the following phases: saturation, consolidation, and static loading.

In the first phase the saturation was tested by determining the coefficient $B = d_u/d_\sigma > 0.96$. This was a relatively short-term phase because of the saturation in the natural state.

The saturated sample was consolidated at the selected effective isotropic consolidation stress σ'_{3c} . The effective isotropic consolidation stress is expressed as the difference in the cell pressure σ_{3c} and the back pressure u_b .

Static loading was performed so that the sample was loaded with the selected compression $d\sigma_{3c}$ or the axial stress $\sigma_a = \sigma_z$.

The following dynamic strength parameters were calculated: the Young's modulus E , the shear modulus G , and the damping ratio ζ . An investigation of the influence of density (in effect, porosity) on the increase in strain and pore pressure was performed.

4 BASIC CHARACTERISTICS

The geomechanical properties of snail soils with different porosities were determined. The snail soil was saturated and treated as a two-phase material (particles and pore water). The chemical and mineral compositions were constant with density, only the volume of water in the pores was changed. The particle size distribution and remains of micro-organisms in snail soil are also constants. In contrast, the specific surface is independent of porosity.

The visual appearance of the snail-soil samples was only tested in the natural state and after static loading.

The parameters of the physical characteristics (Table 1) are constants. The density ρ or the unit weight γ , the void ratio e and the volume strain ε_{vol} are in the well-known correlation. The initial void ratio e_0 is extremely high and the snail soil is at the liquid limit state.

5 STATIC LOADING BEHAVIOUR

The results of previous investigations [4] have shown the relationship between the permeability coefficient k and void ratio e_c . This relationship can be expressed as follows:

$$k(e) = 4 \cdot 10^{-11} \cdot e_c^{5.50} \quad (1)$$

Equation (1) is similar to Eq. (2), which was previously proposed by Dolinar and Žnidaršič for fine-grained soils [5].

$$k(e) = \alpha \cdot e^\beta \quad (2)$$

In Eq. (2) α and β are soil-dependent coefficients.

We can express in a similar way the relationships for the coefficient of consolidation c_v vs. the void ratio e_c . We obtained the expression for the coefficient of consolidation c_v (m²/s):

$$c_v(e) = 3 \cdot 10^{-8} \cdot e_c^{1.46} \quad (3)$$

The relationship of the coefficient of volume compressibility m_v (kPa⁻¹) vs. the void ratio e_c is expressed in a similar way.

$$m_v(e) = 9 \cdot 10^{-5} \cdot e_c^{3.5} \quad (4)$$

An insufficient number of tests were performed to determine the relationship between the strength parameters and the void ratio, and therefore the results were unreliable. The strength did not increase substantially with the decreasing porosity, in fact a greater difference can only be seen for the larger changes of porosity. The relationship between the Young's modulus E (kPa) and the void ratio e_c can be expressed as:

$$E(e) = 7700 \cdot e_c^{-3.15} \quad (5)$$

The ratio between the Poisson's ratio ν and the void ratio e_c is almost linear. The value of the Poisson's ratio is $\nu = 0.4$ at a void ratio of $e_c = 2.0$, and it decreases to a value $\nu = 0.37$ at the plastic limit (the void ratio $e = 1.6$).

The same is true for the shear properties. We can see that they increase almost linearly for smaller changes of the void ratio. The relationship between the friction angle φ (°) and the void ratio e_c is expressed as:

$$\varphi(e) = 39,58 \cdot e_c^{-0.92} \quad (6)$$

6 CYCLIC LOADING BEHAVIOUR

The saturated specimens were consolidated to a particular effective isotropic consolidation stress σ'_0 , expressed as the difference between the cell pressure σ_0 and the back pressure u_b .

The cyclic loading in the undrained conditions was performed with a particular frequency f and an axial cyclic stress σ_d . The axial loading σ_d is a deviator component of the stress, and it has a sinusoidal form with respect to time. The cyclic stress ratio CSR is expressed as:

$$CSR = \frac{\sigma_d}{2\sigma_0} \quad (7)$$

The initial void ratio e_0 and the void ratio after each consolidation e_c were calculated as:

$$e_0 = \frac{\gamma_s}{\gamma_d} - 1 ; \quad e_c = e_0 - \frac{\Delta V}{V_0} \frac{\gamma_s}{\gamma_d} \quad (8)$$

where V_0 is the initial volume of the specimen, ΔV is the volume change, and γ_s , and γ_d are the unit weight and the dry unit weight.

The mechanism of the generation of pore-water pressure due to the cyclic loading in the undrained conditions was used [6]. Due to a particular number of cyclic loadings, a change in the void ratio Δe of the soil occurs if full drainage is allowed. However, if drainage is prevented, the void ratio will remain as an initial effective stress σ'_0 , and will be reduced with an increase in the pore-water pressure Δu . If the number of cycles and the load level is large enough, the magnitude of Δu can become equal to σ'_0 and, in such a case, the soil will liquefy.

The axial strain $\varepsilon_1 = \Delta H/H$ is expressed as a sum

$$\varepsilon_1 = \varepsilon_{1,r} + \varepsilon_{1,p} \quad (9)$$

where ε_r is the recovery part of strain and ε_p is the permanent part of the strain. The recovery part of the strain is calculated as a half of the double amplitude axial strain $\varepsilon_{da}(t)$:

$$\varepsilon_{1,r}(t) = \frac{\varepsilon_{1,max}(N(t)) - \varepsilon_{1,min}(N(t))}{2} = \frac{\varepsilon_{da}(t)}{2} \quad (10)$$

where $N(t)$ is the cycle number at the time t , and $\varepsilon_{1,max}(N(t))$ and $\varepsilon_{1,min}(N(t))$ are the maximum and minimum values of the deformation. The increase of the double amplitude axial strain depends on the initial effective stress, the porosity and the cyclic loading. Fig. 2 (see next page) shows typical relationships for the double amplitude axial strain ε_{da} vs. the number of cycles N .

The permanent part of the strain is calculated as a medium value between $\varepsilon_{1,max}$ and $\varepsilon_{1,min}$ for every cycle. The test result shows a constant and almost zero value of $\varepsilon_{1,p}(t)$.

$$\varepsilon_{1,p}(t) = \frac{\varepsilon_{1,max}(N(t)) + \varepsilon_{1,min}(N(t))}{2} \approx 0 \quad (11)$$

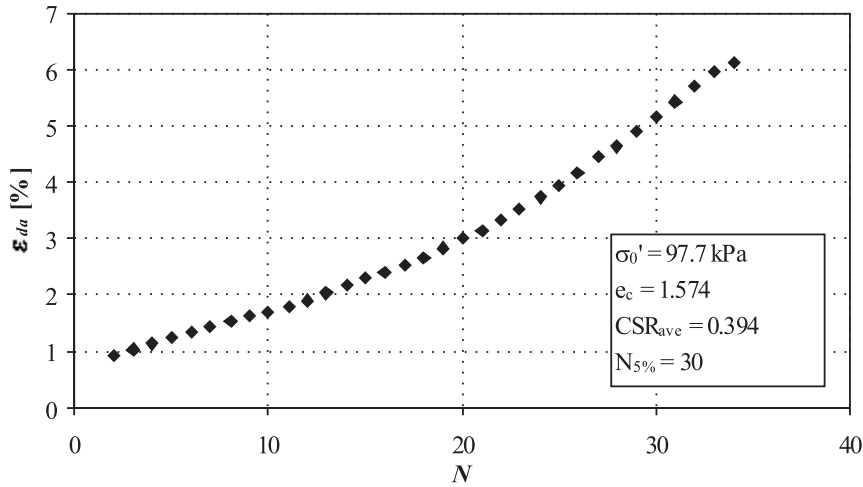


Figure 2. Double amplitude axial strain ϵ_{da} vs. the number of cycles N .

The undrained test is made with the volume strain $\epsilon_v(t) = 0$ and the Poisson's ratio $\nu = 0.5$. The relationships between the cyclic stress σ_d and the shear strain γ can be expressed with a hysteresis loop (Fig. 3)

The damping ratio ξ is derived from the given hysteresis loop and is defined as the ratio between the dissipated energy and the energy used in the deformation. It can be calculated from the ratio between the areas ΔW and W .

$$\xi = \frac{\Delta W}{2\pi W} \quad (12)$$

where ΔW is the area of the cyclic loop and W is the area of the triangle $O - \sigma_d - \gamma$. The deviator stress σ_d is constant and the shear strain γ increases with the number of cycles. The dissipated energy ΔW can be calculated for each cycle as:

$$\Delta W = \frac{1}{2} \sum_{t=0}^T (\sigma_d(t - t_{\sigma_d} + \Delta t) + \sigma_d(t - t_{\sigma_d})) (d\epsilon(t + \Delta t) - d\epsilon(t)) \quad (13)$$

where t is the time, t_{σ_d} is the time at the maximum deviator stress σ_d , Δt is the time increment and T is a period ($T = 1s$).

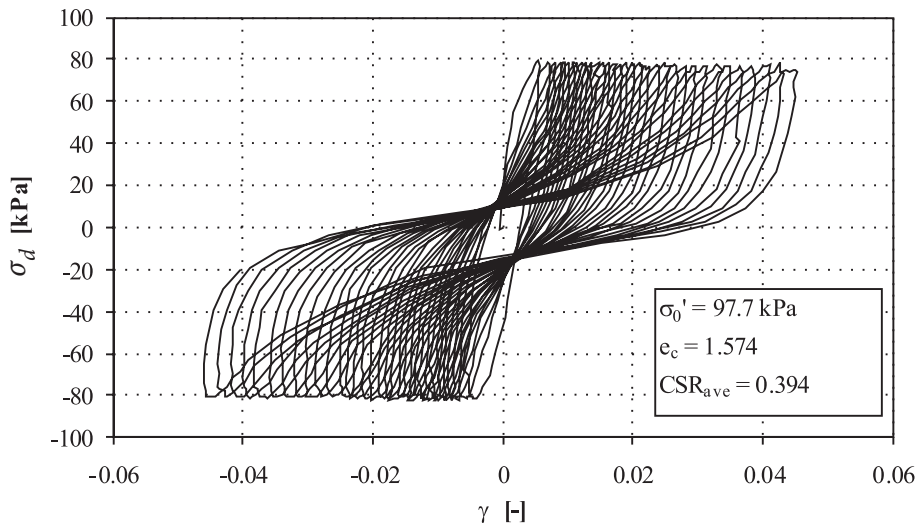


Figure 3. Deviator stress σ_d vs. shear strain γ .

The cyclic loading $\sigma_d(t)$ has a sinusoidal form in each test. The axial strain ε_1 has a sinusoidal form in the first cycles, and after that the part of the plastic strain $\Delta\varepsilon_{1,pl}/\varepsilon_1$ increases with the number of cycles N ; it depends on the cyclic stress ratio CSR and the void ratio e . Fig. 4 shows the part of plastic strain $\Delta\varepsilon_{1,pl}/\varepsilon_1$ after 10 cycles, for the void ratio $e = 1.6$ and for different cyclic stress ratios (CSR s).

The increasing of the pore pressure (Fig. 5) can also be separated into the recovery and permanent parts of the pore pressure [7]. It can, for instance, be expressed with the pore-pressure ratio r_u , as the relationship between

the pore-pressure change Δu and the effective isotropic consolidation stress σ'_0 ,

$$r_u = \frac{\Delta u}{\sigma'_0} \quad (14)$$

Due to ground shaking during an earthquake, a cyclic shear stress is imposed on the soil element. A laboratory test to study the liquefaction problem must be designed in a manner so as to simulate the condition of a constant normal stress and a cyclic shear stress on a plane of the soil specimen. As the actual triaxial tests can be conducted by applying a cyclic load in the axial direction only, corrected cyclic pore-pressure ratios $r_{u,corr}$ are used.

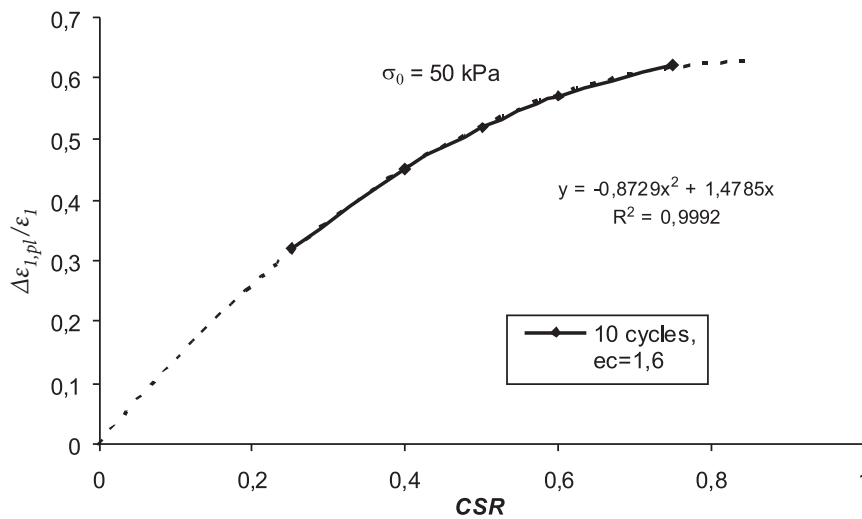


Figure 4. Plastic strain $\Delta\varepsilon_{1,pl}/\varepsilon_1$ vs. the cyclic stress ratio (CSR).

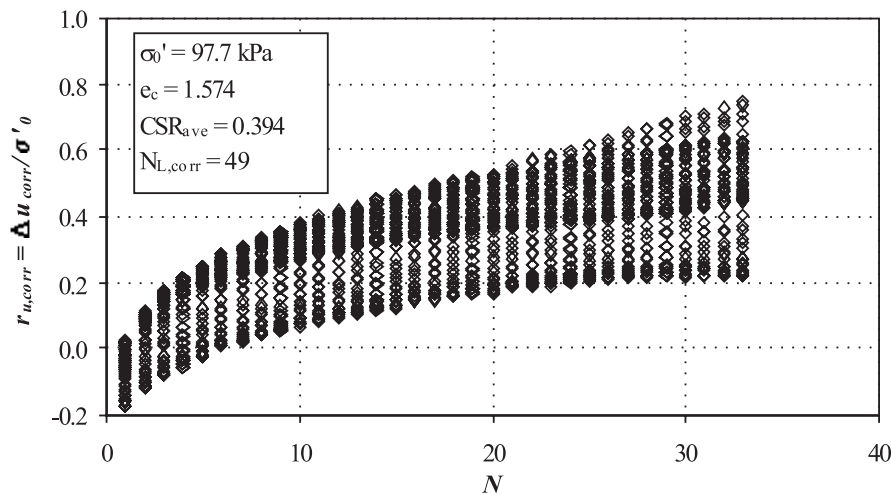


Figure 5. Corrected pore-pressure ratio $r_{u,corr}$ vs. the number of cycles N .

The corrected cyclic pore-pressure ratio $r_{u,corr}$ is expressed as:

$$r_{u,corr} = \frac{\Delta u_w - \frac{\sigma_a}{2}}{\sigma'_0} = r_u - CSR \quad (15)$$

The total change of the pore-pressure ratio r_u is:

$$\begin{aligned} r_u(t) &= r_{u,pov}(t) + r_{u,nepov}(t) \\ r_{u,r}(t) &= \frac{r_{u,max}(N(t)) - r_{u,min}(N(t))}{2} \\ r_{u,p}(t) &= \frac{r_{u,max}(N(t)) + r_{u,min}(N(t))}{2} \end{aligned} \quad (16)$$

where $r_{u,r}$ is the recovery part of the pore-pressure ratio and $r_{u,p}$ is the permanent part of the pore-pressure ratio. The ratios $r_{u,max}$ and $r_{u,min}$ are the maximum and minimum measured values of r_u in the cycle $N(t)$.

The recovery part of the pore pressure is a consequence of the transfer of pressure to the pore water and it is present as long as the cyclic loading continues. The permanent part of the pore pressure is a consequence of the volume change and the removal of particles because of the cyclic shear stress. The permanent part of the pore-pressure ratio $r_{u,p}$ increases with the number of cycles N and it is dependent on the cyclic stress ratio CSR and the void ratio e_c . The recovery part of the pore pressure, already during the first cycle, increases the hydrostatic part of the cyclic loading to $u(N=1) \geq \sigma_d/3$ or more (depending on the CSR).

The strain and the pore-pressure increases correlate well and depend on the initial stress σ'_0 , the cyclic stress ratio (CSR) and the void ratio e_c . Fig. 6 shows the relationship for the corrected cyclic pore-pressure ratio $r_{u,corr}$ vs. the shear strain γ .

Fig. 7 shows the number of cycles N for the various void ratios e_c needed to reach some value of the pore-pressure ratio r_u and for constant values of the cyclic stress ratio (CSR) and the initial effective stress σ'_0 . It is evident that increasing the pore pressure is independent of the void ratio e_c until it reaches some value of the pore-pressure ratio ($r_u > 0.7$).

The relationship between the number of cycles N and the void ratio e_c in order to reach some value of the shear strain γ is similar. Fig. 8 shows such a relationship for the constant values of the cyclic stress ratio CSR = 0.39 and the initial effective stress $\sigma'_0 = 100$ kPa. The increase of the shear strain becomes dependent on the void ratio when it reaches some value of the shear strain ($\gamma > 0.3$).

The damping ratio ξ in stress-controlled tests shows an initial increasing of the curve with the increasing strain deformation and the number of cycles. The shape of the curve (Fig. 9) shows an exponential increase with the increase of the shear strain, up to a strain of about 0.5%. With greater strains, the damping ratio is constant and after that the values exponentially fall and appear to reach an asymptotic value. This phenomenon is due to the loss of shear strength because of the effective stress approaching zero and the material being about to liquefy. Similar behaviour for the damping ratio ξ has been observed in lacustrine carbonate silt from the

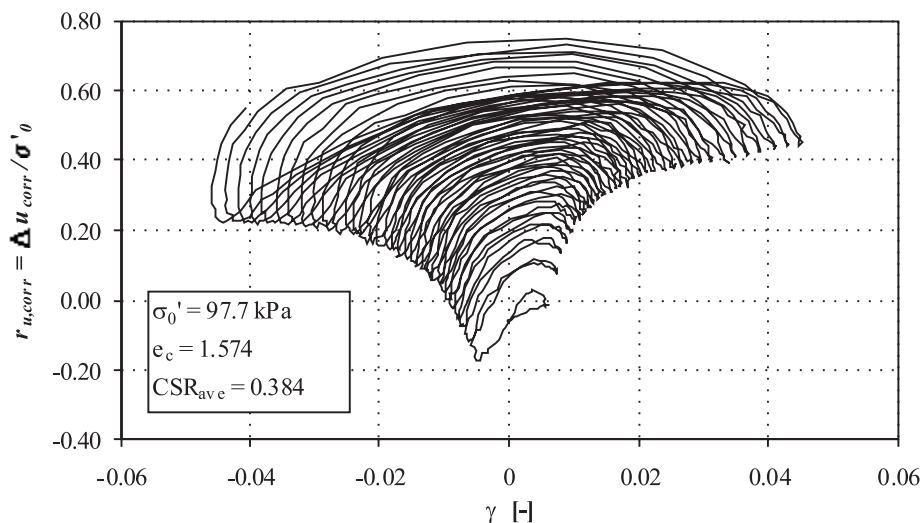


Figure 6. Pore-pressure ratio $r_{u,corr}$ vs. shear strain γ .

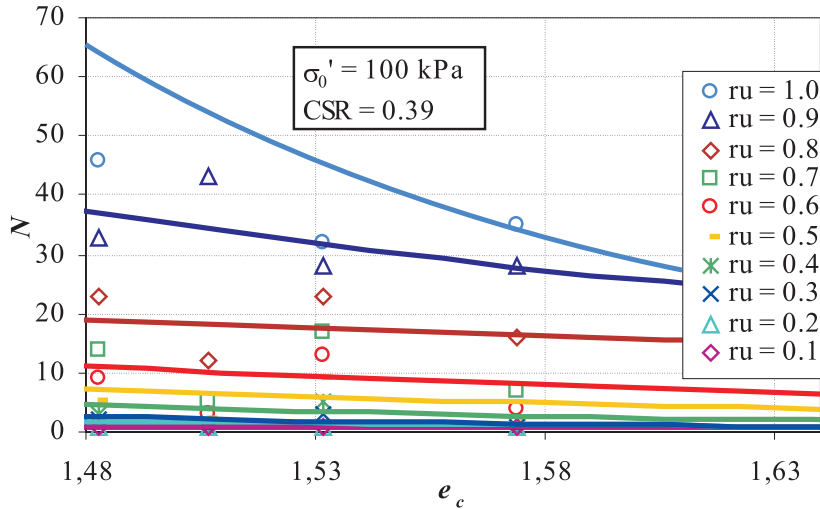


Figure 7. Number of cycles N_{ru} vs. the void ratio e .

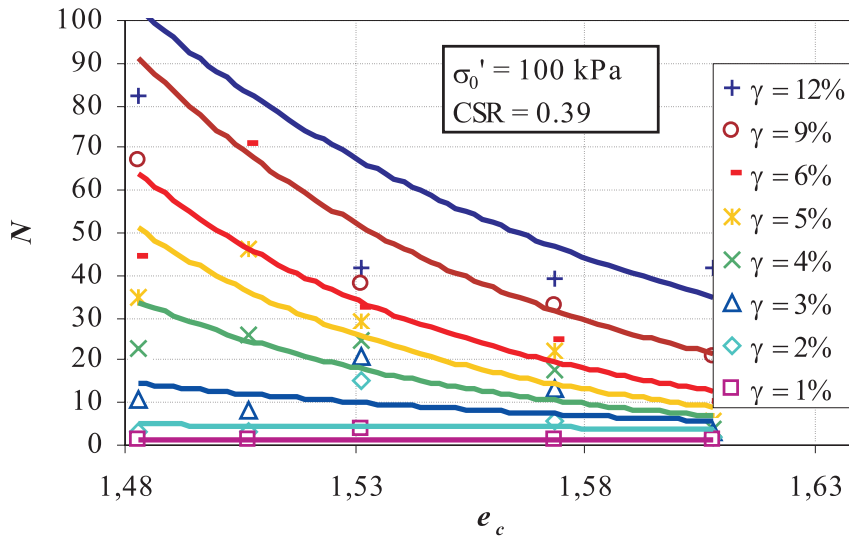


Figure 8. Number of cycles N_{γ} vs. the void ratio e .

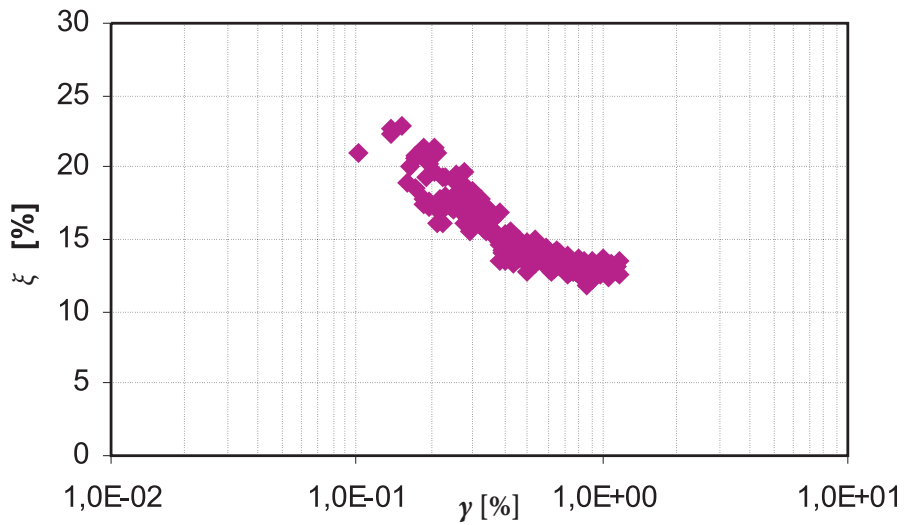


Figure 9. Damping ratio ξ vs. the shear strain γ .

Julian Alps [8]. The strain and the maximum value of ξ are different, but the shapes of the curve describing the phenomenon are similar.

Figure 10 shows the maximum and the asymptotic values of the damping ratio ξ for the different initial effective stress conditions σ'_0 and the void ratio e_c . It is evident that the porosity does not influence the damping ratio ξ during larger strains.

The shear modulus G and the Young's modulus E are described in relation to the shear strain γ and to the axial

strain ε_1 . The impact of the initial effective stress on the shear modulus across a large strain range is shown in Fig. 11.

Fig. 12 shows the relationship between the shear modulus G and the void ratio e_c after 10 cycles and for different cyclic stress ratios (CSRs) and for an initial effective stress $\sigma'_0 = 50$ kPa. It is evident that porosity influences the shear modulus, but only for higher values of the cyclic stress ratio (CSR).

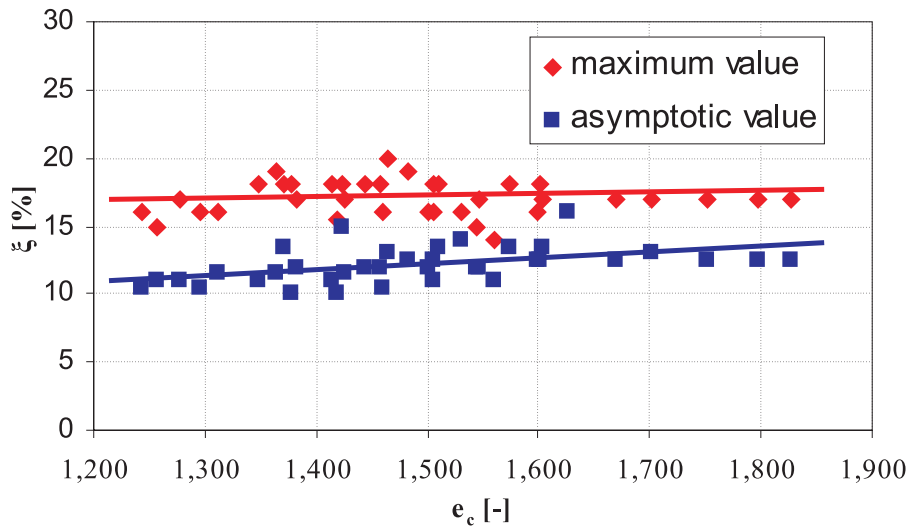


Figure 10. The range of limit values for damping ratio ζ with respect to the void ratio e_c .

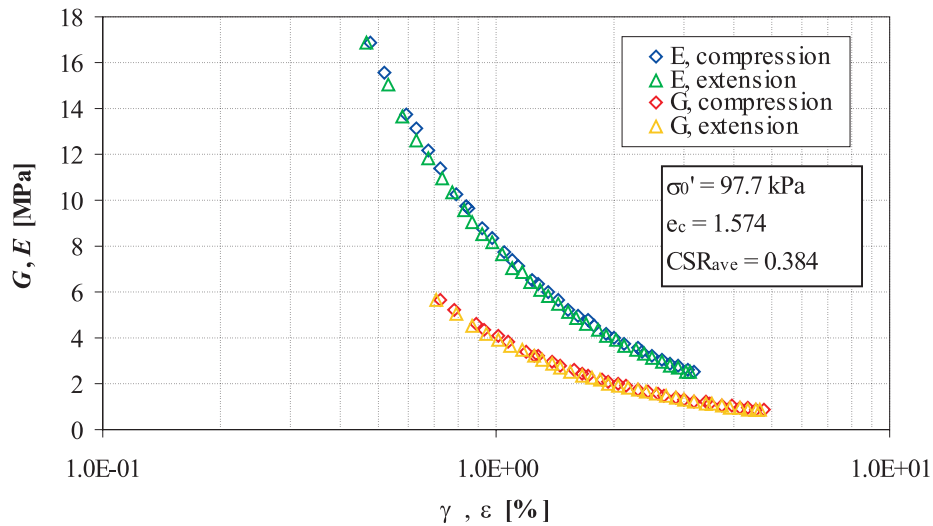


Figure 11. Young's modulus E vs. the axial strain ε_1 , and shear modulus G vs. the shear strain γ .

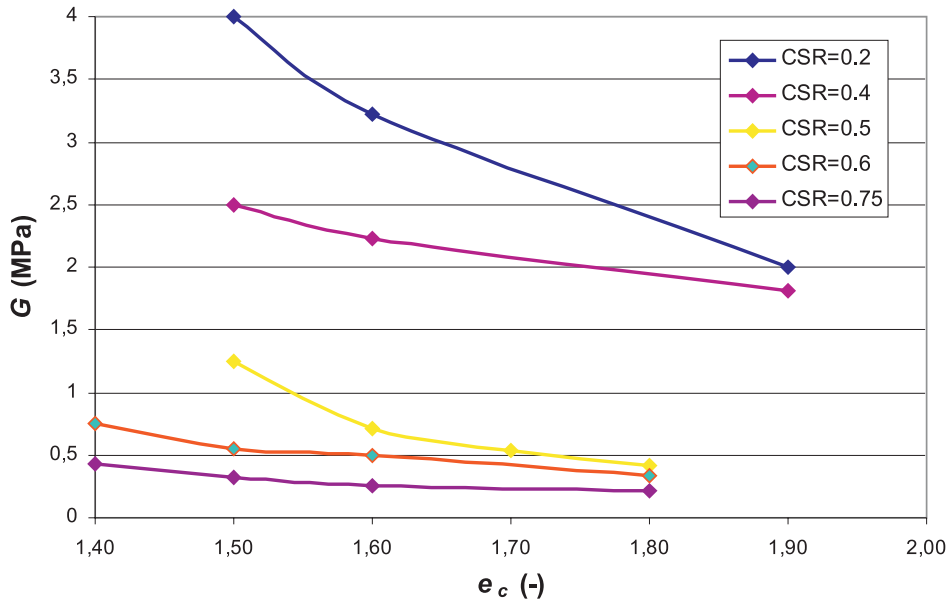


Figure 12. Shear modulus G versus the void ratio e_c at an initial effective stress $\sigma'_0 = 50$ kPa and for various cyclic stress ratios (CSRs), after 10 cycles.

The axial and shear strain γ increase with the number of cycles N depending on the initial effective stress σ'_0 and the cyclic stress σ_d (or the cyclic stress ratio CSR). The cyclic stress σ_d , the cyclic stress ratio CSR and the shear modulus G can be expressed for each initial effective stress σ'_0 and for a selected value of the shear strain γ . Fig. 13 shows the relationship between the cyclic stress ratio CSR and the void ratio e_c for a shear strain γ after 10 cycles and for different initial effective stresses σ'_0 .

Fig. 14 shows the similar relationship between shear stress τ and the effective stress $\sigma'_0 = 50$ kPa for the shear strain $\gamma = 7.5\%$ after 10 cycles. It is expressed for different initial effective stresses σ'_0 and for different void ratios e_c . It is evident that the relation $\tau - \sigma'_0$ is linear and expresses the failure lines of the snail soil for different void ratios e_c . The relationship shear stress τ vs. effective stress σ'_0 for smaller values of shear strain γ is similar and represents the deformation lines.

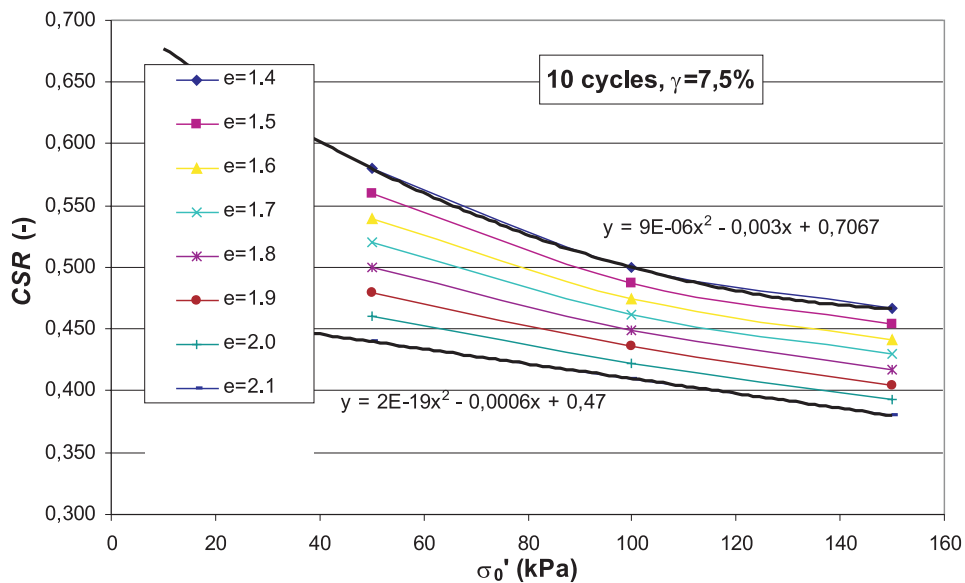


Figure 13. Cyclic stress ratio CSR versus the void ratio e_c for a shear strain $\gamma = 7.5\%$ after 10 cycles.

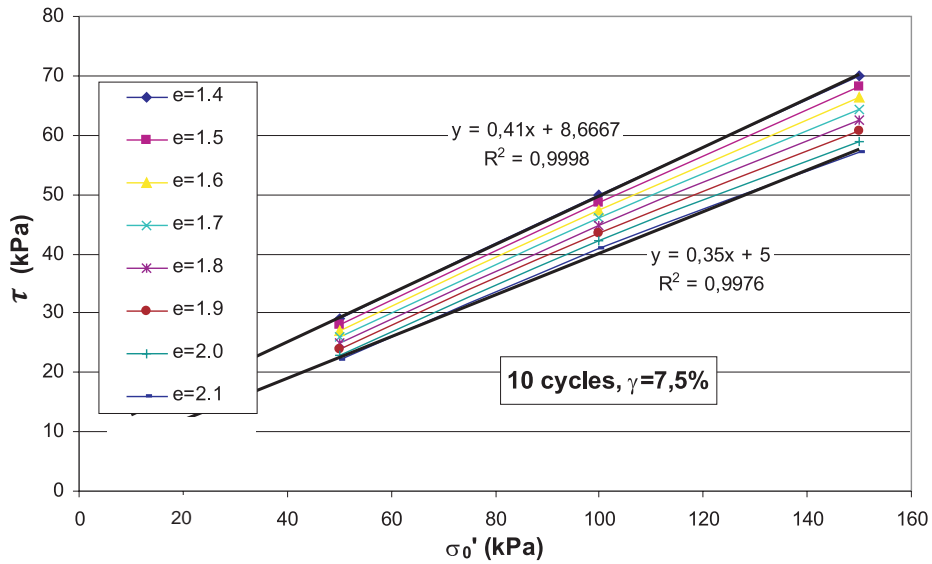


Figure 14. Shear stress τ versus the effective stress $\sigma'_0 = 50$ kPa for a shear strain $\gamma = 7.5$ %.

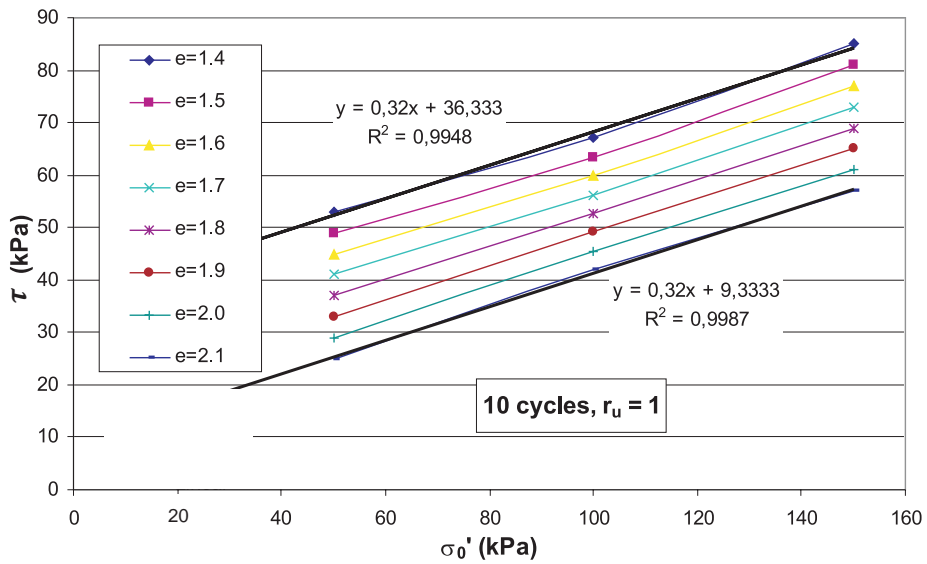


Figure 15. Shear stress τ versus the effective stress $\sigma'_0 = 50$ kPa at a pore-pressure ratio $r_u = 1$.

Fig. 15 shows the relationship between the shear stress τ and the effective stress σ'_0 for a pore-pressure ratio $r_u = 1$ and for various void ratios e_c after 10 cycles. Such a relationship is also linear (except for small values of the effective stress $\sigma'_0 < 20$ kPa and the express failure lines of the snail soil at various void ratios e_c using the pore-pressure criteria).

The relationships between the shear stress τ and the effective stress σ'_0 for values of the pore-pressure ratio $r_u < 1$ are expressed similarly.

By comparing both criteria, it is clear that the snail soil is a highly sensitive material. For low values of the effective stress σ'_0 (under the surface) the large strain results in failure; however, at higher values of the effective stress σ'_0 (deeper under the surface) failure arises as a consequence of a high pore pressure.

7 CONCLUSIONS

The geomechanical characteristics of snail soil were investigated for their dependence on the physical characteristics. A series of tests with different porosities was performed. The test results show that the geomechanical characteristics depend on the porosity. It is evident from the results that the changes in the coefficient of permeability, the coefficient of consolidation, and the coefficient of volume compressibility are non-linear with respect to the changes in the porosity. The initial changes (at high porosity) are higher than the changes at low porosity.

The changes of the mechanical parameters, such as the Young's modulus, the Poisson's ratio, and the friction angle are indistinct and almost linear for smaller changes of porosity, but become non-linear for larger changes of porosity.

The snail soil was recognized as being a highly sensitive material. A large strain appears after the initial cycles.

The pore pressure increased even during the first cycle to the hydrostatic part of cyclic loading, or higher (depending on the CSR).

The damping ratio increased exponentially with the strain, and after some cycles reached its maximum value, and after that decreased to an asymptotic value. The reason for such behaviour is the large plastic deformation. The maximum and asymptotic values of the damping ratio are changed only minimally with the void ratio. There is clearly no influence of the porosity on the damping ratio.

The shear modulus G and the Young's modulus E are described in relation to the shear strain γ and to the axial strain ε_1 . The porosity influences the shear modulus only at higher values of the cyclic stress ratio (CSR).

The increase of the pore pressure is independent of the void ratio e_c until it reaches some value of the pore pressure ratio ($r_u > 0.7$). Similarly, the increase of the shear strain becomes dependent on the void ratio until it reaches some value of the shear strain ($\gamma > 0.3$).

The deformation and failure lines are determined from the relationship between the shear stress τ and the effective stress σ'_o at some shear strain γ after 10 cycles. The limit value of the shear strain is $\gamma = 7.5\%$.

The relationships between the shear stress τ and the effective stress σ'_o for values of the pore-pressure ratio $r_u < 1$ are expressed similarly. Such a relationship is linear (except for small values of the effective stress

$\sigma'_o < 20$ kPa and express pore-pressure lines of snail soil at different void ratios e_c using pore-pressure criteria and a failure line when the pore pressure ratio $r_u = 1$).

ACKNOWLEDGMENTS

This research is part of a three-year research project financed by the Slovenian Ministry of Higher Education, Science and Technology. The financial support of the company Prevent and the Slovenian Road Operator, DARS, is also gratefully acknowledged.

REFERENCES

- [1] Trauner, L. (1982). *Applicability of theory of elasticity for foundation design*. Doctoral thesis, University of Ljubljana, Ljubljana.
- [2] Trauner, L. et al. (1982). Structure soil interaction, *Research report*, University of Maribor, 67, Maribor.
- [3] Žlender, B. et al. (2007). Cyclic triaxial tests of soil, *Research report*, University of Maribor, Maribor.
- [4] Žlender, B., Trauner, L. (2006). The influence of porosity on geomechanical characteristics of snail soil in the Ljubljana marsh. *Acta Geotechnica Slovenica*, Vol. 3, No. 1, 34-42.
- [5] Dolinar, B. and Žnidaršič, M. (2007). Evaluation of permeability of saturated clays based on their physical properties. *Geologija* 50, 2 487-495.
- [6] Das, B.M. (1993). Principles of soil dynamics, *PWS-KENT Publishing Company*, 397-453.
- [7] Lenart, S. (2005). *Numerical model for calculation pore pressure in soils with high liquefaction potential*. Doctoral thesis. University of Ljubljana.
- [8] Žlender, B. and Lenart, S. (2005). Cyclic liquefaction potential of lacustrine carbonate silt from Julian Alps. *Acta Geotechnica Slovenica*, Vol. 2, No. 1, 22-31.